Characterization and design of micro-photonic devices and optical metamaterial with full wave simulations

Sy-Bor Wen, Arun Bhaskar, Vijay M. Sundaram Department of Mechanical Engineering, Texas A&M University, College Station, TX 77843

Introduction

When the characteristic length of the objective is comparable or less than the wavelength of the light, wave behaviors of light becomes important, which cannot be properly described with traditional ray optics. In addition to light interference and diffractions, wave behaviors such as near field light scattering, evanescent field generation, surface plasmon/phonon stimulation, and localized plasmon resonance can happen at this small length scale. In other words, wave optical analysis is commonly required to determine the micro-nanoscale light-material interaction as well as the design of new optical material composed with micro-nanoscale structures. In this poster, we summarized a portion of our previous work relating to the utilization of wave optics to determine the performance of micro-nano optical devices as well as the design of optical metamaterial to achieve perfect light absorption. The presentation is divided into three groups (a) nanoscale light focusing by teardrop scatterer; (b) optical energy transport in NSOM probes, and (c) design of perfect light absorber (at mid-IR range). All the results are mainly obtained from solving Maxwell's equations directly. Since the mesh size in full wave simulation with Maxwell's equations should be less than ~$\lambda/4$ to ~$\lambda/10$, more than a few millions of meshes is commonly required even for a small domain full wave simulation. Therefore, to perform these large scale simulation, we mainly rely on EOS and ADA clusters at TAMU especially for cases requiring parametric distributed parallel simulations. Much of simulations were done using Comsol with 20 processor cores and 600 GB memory.

Sy-Bor Wen, Arun Bhaskar, Vijay M. Sundaram Department of Mechanical Engineering, Texas A&M University, College Station, TX 77843

Theory

The numerical results presented in the following sections are based on solving the following two governing equations under 2D evolutionally symmetric or 3D conditions with either finite different finite element method (FEM).

(a) Wave optical simulation with Maxwell's equations in frequency domain

$$\nabla \cdot \vec{D} = 0; \quad \nabla \cdot \vec{B} = 0; \quad \nabla \times \vec{E} = -j\omega\mu_0\vec{H}; \quad \nabla \times \vec{H} = -j\omega\varepsilon_{r0}\varepsilon_0\vec{E}$$

where $\vec{E}$, $\vec{D}$, $\vec{B}$ and $\vec{H}$ are the electric field, electric displacement, magnetic induction and magnetic field in the frequency domains; ε_r is the relative permittivity of the material, ε_0 is the permittivity of free space; μ_0 is the permeability of the material. The induced current density is $\vec{J} = j\omega\vec{D}$. The time average joule heating φ is $\frac{1}{2}\mathrm{Re}(-j\omega E \cdot D^*)$.

(b) Heat transfer simulation with two temperature model for the heat diffusion in the solid

$$C_e \frac{\partial T_e}{\partial t} = \varphi + \nabla \cdot (K_e \nabla T_e) - \frac{C_e}{\tau_{e-p}}(T_e - T_p) \qquad C_p \frac{\partial T_p}{\partial t} = \varphi + \nabla \cdot \left(K_p \nabla T_p\right) - \frac{C_p}{\tau_{e-p}}(T_e - T_p)$$

where C_e and C_p are the heat capacity of electrons and phonons, respectively; T_e and T_p are the electron and phonon temperatures, respectively; K_e and K_p are electron and phonon conductivity, respectively; and τ_{e-p} is the relaxation time between the electrons and phonons. To reduce the simulation time, the wave optics simulation is decoupled with the heat transfer analysis, which is a good assumption when the light pulse width is much less than the thermal diffusion time constant.

Characterization and design of micro-photonic devices and optical metamaterial with full wave simulations

Sy-Bor Wen, Arun Bhaskar, Vijay M. Sundaram
Department of Mechanical Engineering, Texas A&M University, College Station, TX 77843

Nanometer focusing by teardrop scatterer

Most of micro-nano optical devices require metal structures to confine light to a nm spot through evanescent wave generation and/or stimulation of surface/localized plasmon resonance. However, metal structure can cause joule heating which can easily damage the optical device under high energy operation. Therefore, we decided to design a new type of nano-optical device which can focus light to a deep nanoscale spot purely with dielectric components. The approach we developed is based on of cascade light focusing (figure 1): with an appropriate ball lens placed at the end of the optical fiber, the light emitted from the optical fiber can be confiner to a spot ~λ with λ the light wavelength (figure 1a). To reduce a light spot to ~λ/2, a microsphere with a diameter around 5-10 λ can be placed at the focal spot of the ball lens to induced the photonic jet effect (figure 1b). Figure 2 shows the combination of a 58 μm ball lens and a 3 μm microsphere at the focal spot of the ball lens to compress the light from a 10 μm core optical fiber to a ~250 nm spot when λ~400 nm. To further reduce the light spot to sub 100 nm spot, we proposed to place a teardrop scatterer at the photonic jet after the microsphere (figure 1c). The teardrop scatter can be considered as a snowman scatterer (figure 3a) with a filled gap between the top and bottom spheres (figure 3b). The resulting cascade light focusing device as a combination of a ball lens, a microsphere and a teardrop scatterer stacked on the top of a cleaved optical fiber is illustrated in figure 1d.

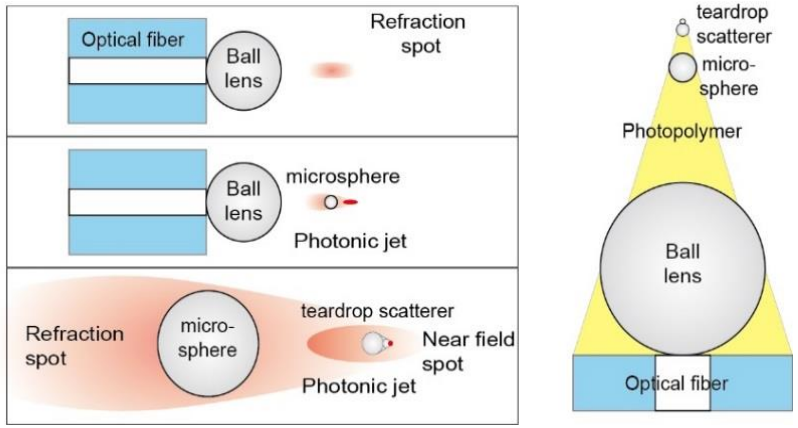

Figure 1: Schematic of deep nm light focusing with cascade light focusing through (a) a ball lens, then (b) a microsphere, and then (c) a teardrop scatterer. The final pure dielectric optical device is illustrated in (d).

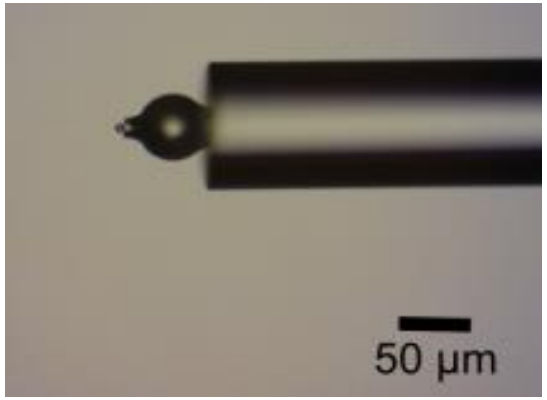

Figure 2: Assembly of a 58 μm ball lens and a 3 μm microsphere at its focal spot to confine the 400 nm light to a ~250 nm spot.

Characterization and design of micro-photonic devices and optical metamaterial with full wave simulations

Sy-Bor Wen, Arun Bhaskar, Vijay M. Sundaram Department of Mechanical Engineering, Texas A&M University, College Station, TX 77843

Nanometer focusing by teardrop scatterer

When both the top and bottom spheres of the teardrop scatterer are made with silica with diameters equal to 500 nm and 10 nm, respectively, we figured out that cascade light focusing can provide a ~5 nm spot at the end of the teardrop scatterer with high local electric field intensity (figure 4). The simulation was conducted with EOS cluster of the TAMU. Each simulation takes about ~800 BU.

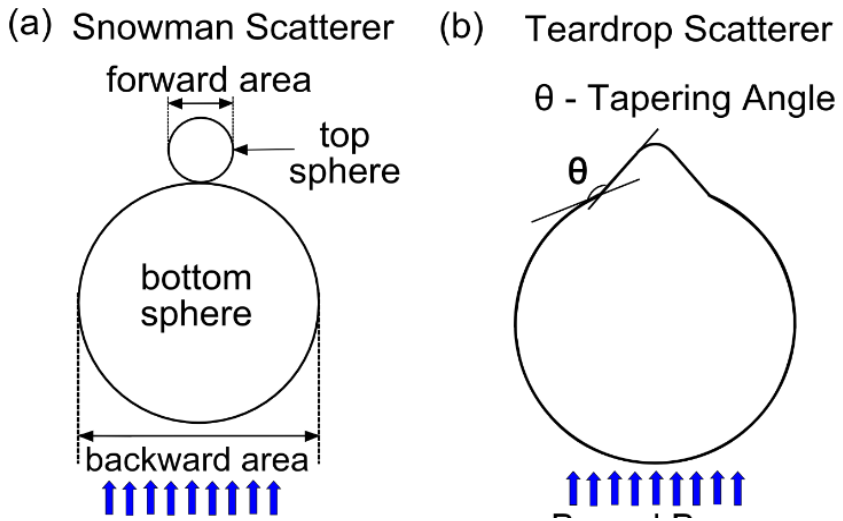

Figure 3: Schematic of a (a) snowman scatterer, and (b) a teardrop scatterer used to confine light to a deep nm spot

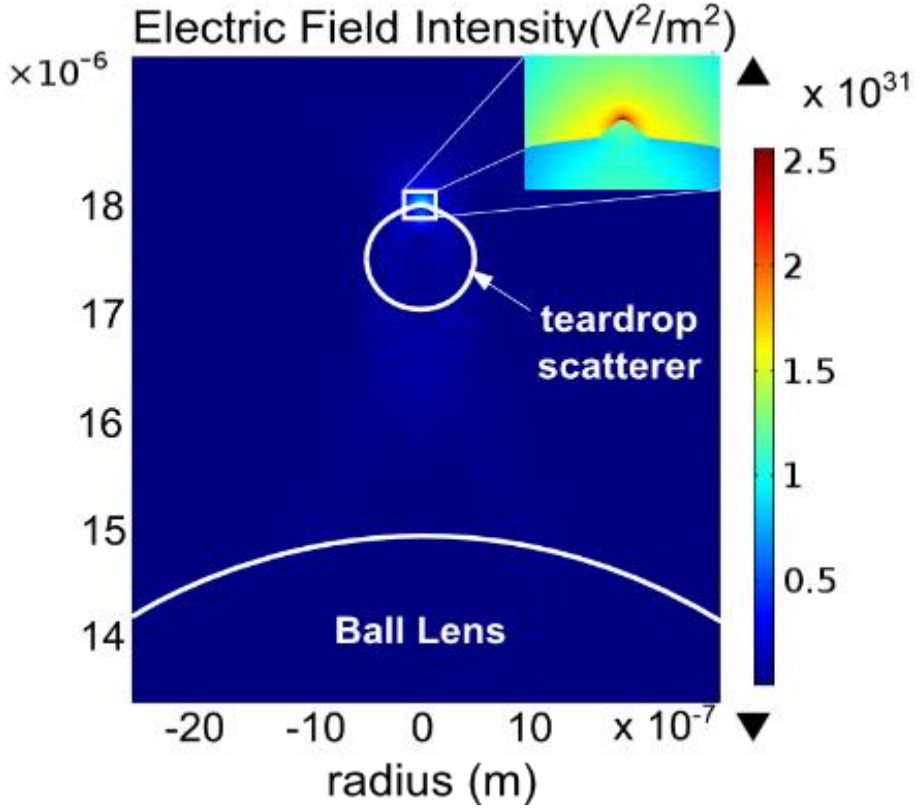

Figure 4: full wave simulation results of ~5 nm light confinement at the forward end of the teardrop scatterer

Sundaram, V. M, Wen, S. B. "Nanoscale high intensity light focusing with pure dielectric non-spherical scatterer," Optics Letters. 39, 2014

Characterization and design of micro-photonic devices and optical metamaterial with full wave simulations

Sy-Bor Wen, Arun Bhaskar, Vijay M. Sundaram Department of Mechanical Engineering, Texas A&M University, College Station, TX 77843

Optical energy transport in NSOM probes

Near field scanning optical microscopy (NSOM), which is broadly utilized in nanoscale detection and analysis, has the ability to break the diffraction limit of light and achieve a spatial resolution down to tens of nm through multiple internal reflections and the associated generation of evanescent waves (figure 5). In traditional NSOM applications, the light intensity conveyed by a NSOM system is limited to a relatively low energy level to prevent damage to the target and to the NSOM probe. Therefore, in most applications relating to NSOM, the heating of the target is small. Recently, people start using NSOM to deliver intense laser pulse to a semi-conductor or metal surface to achieved nm level direct laser machining. Figure 6 shows some experimental results we obtained by coupling a 50 nm apertured NSOM probe with 100 fs laser pulse at λ=400 nm

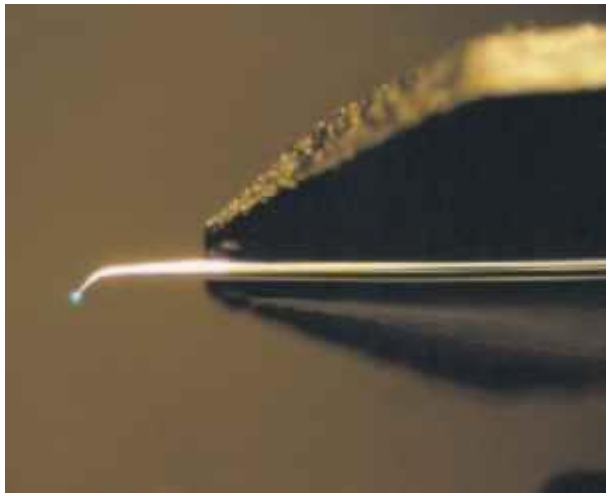

Figure 5. Side view of a NSOM probe with light emitting from the tip at the left end.

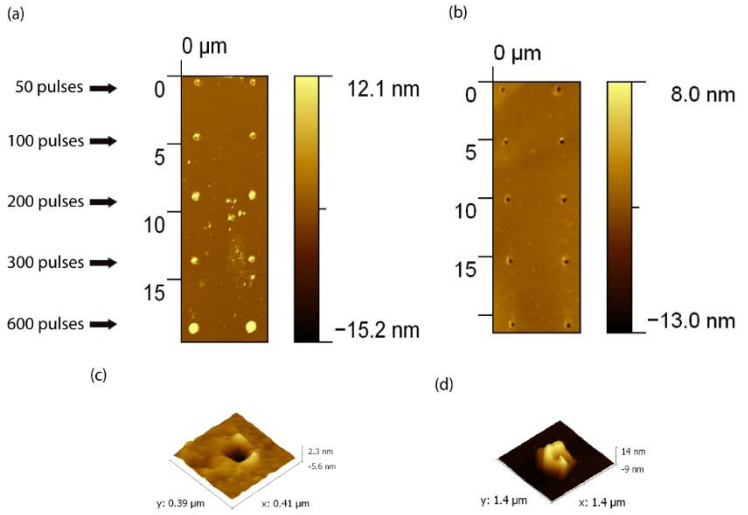

Figure 6. Nano-patterns generated on silicon using femtosecond laser (a) before etching with BHF (b) after etching with BHF (c) after single pulse (d) after 200 laser pulses.

Characterization and design of micro-photonic devices and optical metamaterial with full wave simulations

Sy-Bor Wen, Arun Bhaskar, Vijay M. Sundaram
Department of Mechanical Engineering, Texas A&M University, College Station, TX 77843

Optical energy transport in NSOM probes

For these nm direct laser machining with NSOM, due to the higher input laser energy, NSOM probe can easily be damaged due to high temperature melting and/or exfoliation of the metal coating on the NSOM probe. To better understand the heating in NSOM probes in order to control it in the nm direct laser machining, we have performed full wave simulation to study the light transport in the NSOM probe and the associated heating process. Figure 7 shows the simulated electric field distribution in an NSOM probe under a HE11 mode light illumination

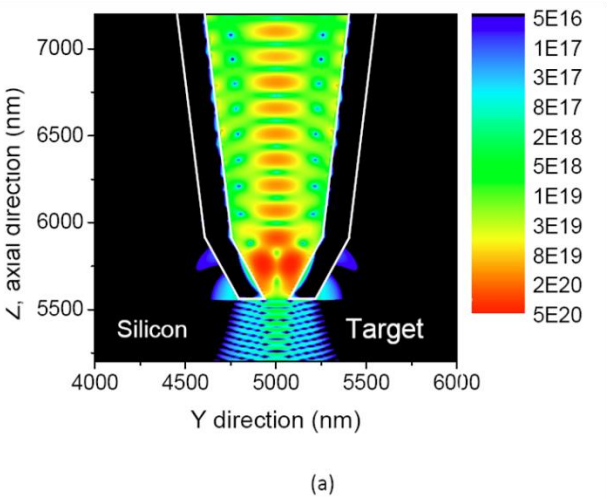

(a)

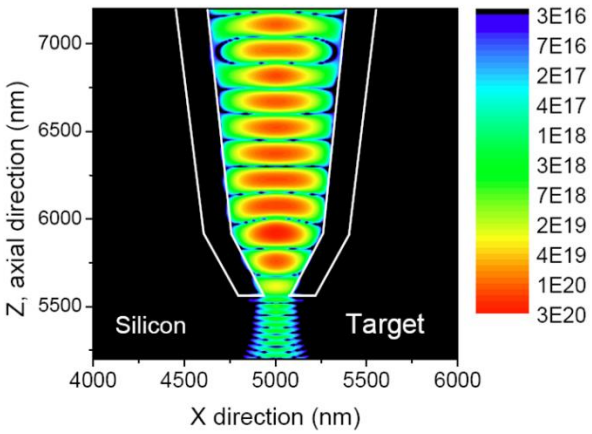

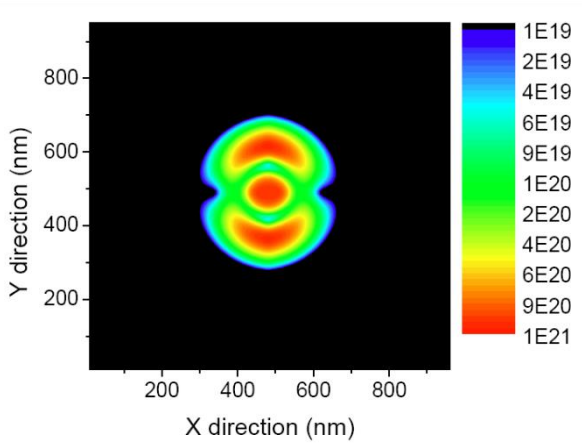

(a)

Figure 7: Spatial distribution of the electric field in the (a) polarization direction, (b) normal to the polarization direction, and (c) end surface of the NSOM probe during a 100 fs laser pulse at 400 nm. The entire simulation domain is illustrated in (d).

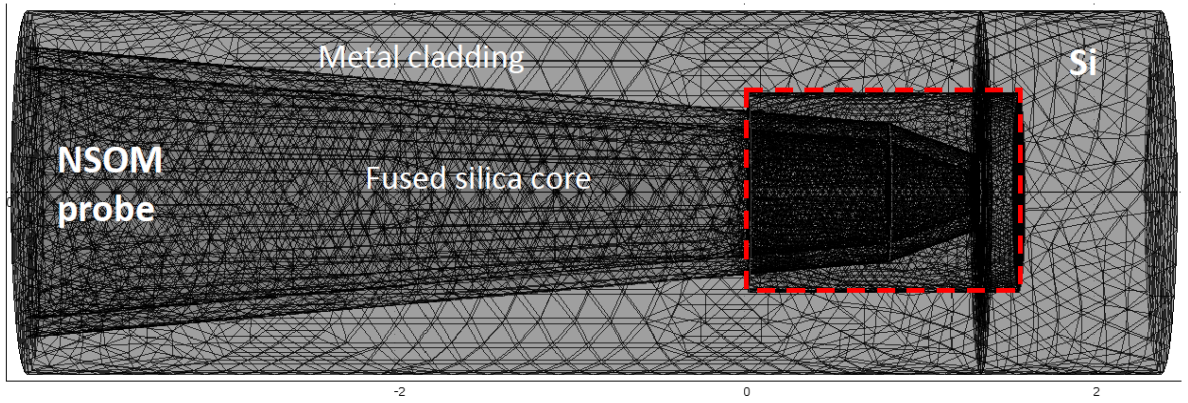

Characterization and design of micro-photonic devices and optical metamaterial with full wave simulations

Sy-Bor Wen, Arun Bhaskar, Vijay M. Sundaram Department of Mechanical Engineering, Texas A&M University, College Station, TX 77843

Optical energy transport in NSOM probes

With the determined electric field and the corresponding joule heating from the formulas described in the theoretical section, we then evaluated the temperature distribution inside the NSOM probe and the adjacent Si target at the end of the laser pulse.

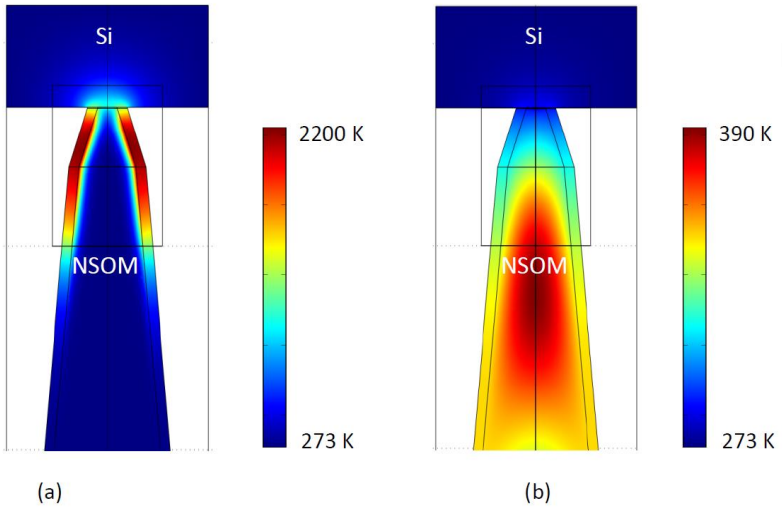

Figure 8: The temperature distribution of the NSOM probe and the Si target at (a) end of the laser pulse, and (b) 100 ns after the laser pulse.

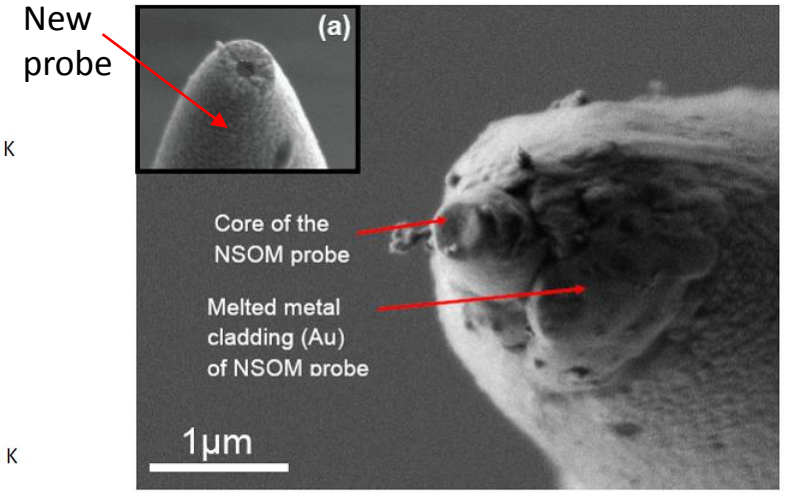

Figure 9: SEM images of a NSOM probe with laser induced melting of the Au coating when E>~2 nJ

As illustrated in the above figure 8, the metal cladding temperature of the NSOM probe is more than the metaling temperature of the (the cladding material of the NSOM probe) at the end of the laser pulse when E = 2 nJ . This explained why we observed the melting of the NSOM probe around the peak temperature region of the figure 8 when E>~2 nJ in our previous experiments (figure 9). The probe temperature decreases rapidly due to conduction to the core of the NSOM probe and the adjacent Si target. In ~100 ns, the probe temperature decrease to only ~100 K higher than the room temperature. To mitigated the extremely high temperature at the metal cladding of the NSOM probe during the fs laser nm direct machining, we also simulated NSOM probes with different tapering angles and different aperture sizes (in the following figure) and have determined that NSOM probe with smaller tapering angle and large aperture size can significantly reduce the joule heating effects.

Characterization and design of micro-photonic devices and optical metamaterial with full wave simulations

Sy-Bor Wen, Arun Bhaskar, Vijay M. Sundaram Department of Mechanical Engineering, Texas A&M University, College Station, TX 77843

Optical energy transport in NSOM probes

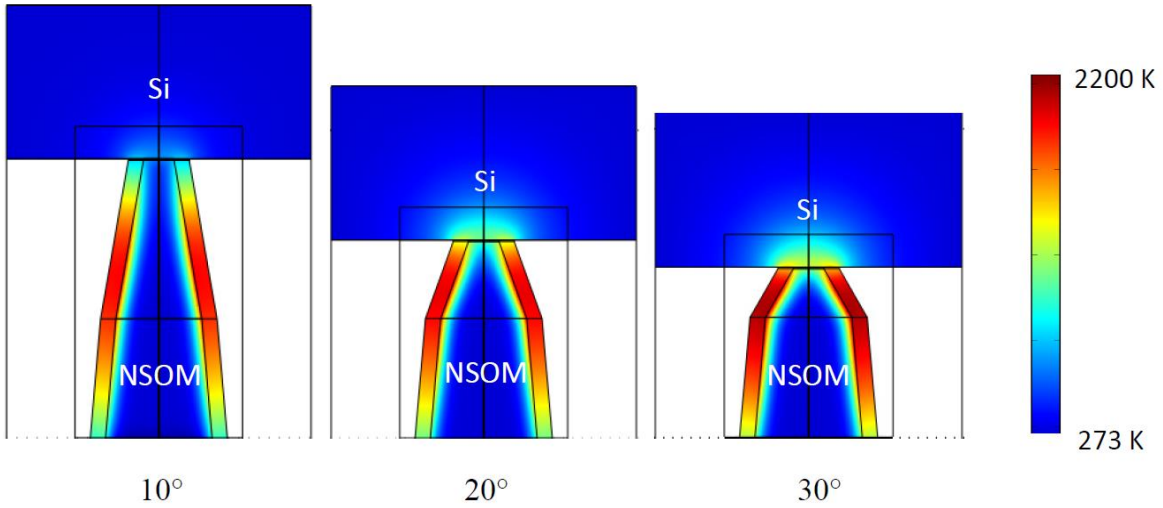

Figure 10: Comparison of the temperature distribution in NSOM probes at the end of 100 fs laser pulse with different tapering angles close to the tip. Each NSOM probe has 100 nm Au cladding . The input light has λ=400 nm and E=2.0 nJ.

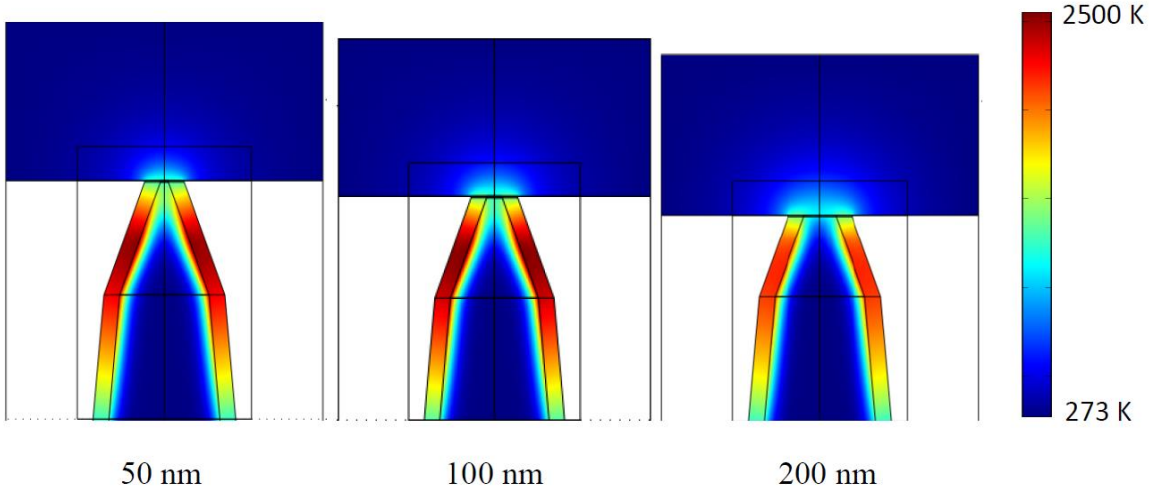

Figure 11: Comparison of the temperature distribution in NSOM probes at the end of 100 fs laser pulse with different aperture size. Each NSOM probe has 100 nm Au cladding . The input light has λ=400 nm and E=2.0 nJ.

However, based on the same sets of simulation, we found that the laser energy transport efficiency shows orders decrement when the tapering angle of the NSOM probe is reduced. In other words, even through the peak temperature of the NSOM probes is reduced, the amount of laser energy can be delivered to the Si target is also reduced when the tapering angle of the NSOM probe is reduced. More laser energy is required to delivered to the NSOM probe with smaller tapering angle, which in turn provides even higher thermal damage of the probe. For reducing the NSOM probe temperature through increasing the aperture size, the main drawback is the resulting decrement of the spatial resolution of NSOM probes in nm laser direct machining.

Wen, S. B., Greif, R., Combined wave based optical analysis and particle based thermal analysis of nanoscale ultrafast target heating of silicon utilizing a near field scanning optical probe and a femtosecond laser, Journal of Physics D, Applied Physics,075502, 2009

Characterization and design of micro-photonic devices and optical metamaterial with full wave simulations

Sy-Bor Wen, Arun Bhaskar, Vijay M. Sundaram
Department of Mechanical Engineering, Texas A&M University, College Station, TX 77843

Design of perfect light absorber

A perfect light absorber is a device which absorbs all the light that incidents upon it at a particular wavelength. A perfect absorber can be achieved with metamaterial composed with micro/nanoscale surface patterns. In this study, we test the performance of perfect light absorber based on a metamaterial constructed with sub-wavelength cross-shaped electric ring resonator (ERR), which is proposed by Willie J. Padilla in 2010. The resulting metamaterial is illustrated in figure 12a as an infinitely large array of metal ERR stacked on a thin dielectric material placed on a metal block. When light with appropriate wavelength strikes the metal cross-shaped ERR, standing electric field with high intensity will be induced in the ERR, which in turn causes strong magnetic field resonance in the dielectric layer confined by the top metallic ERR and the bottom metal base. By adjusting the amplitude of the electric and magnetic resonances, the impedance of the metamaterial can be fine tuned to have zero reflection at selected wavelengths (i.e., perfect absorber). To achieve this critical condition, the size of the ERR and the thickness of the dielectric layer should be well designed. To determine the required size of the ERR when it is made with Au as well as the required thickness of the dielectric layer when it is constructed with alumina to achieved perfect light absorption at λ=6.5 μm, we carried out a batched simulation to test the light absorptivity of this specific type of metamaterial with different sizes of Au cross-shaped ERR and different alumina layer thicknesses with full wave simulation. Figure 12c shows the simulation domain and the results are presented in figures 13.

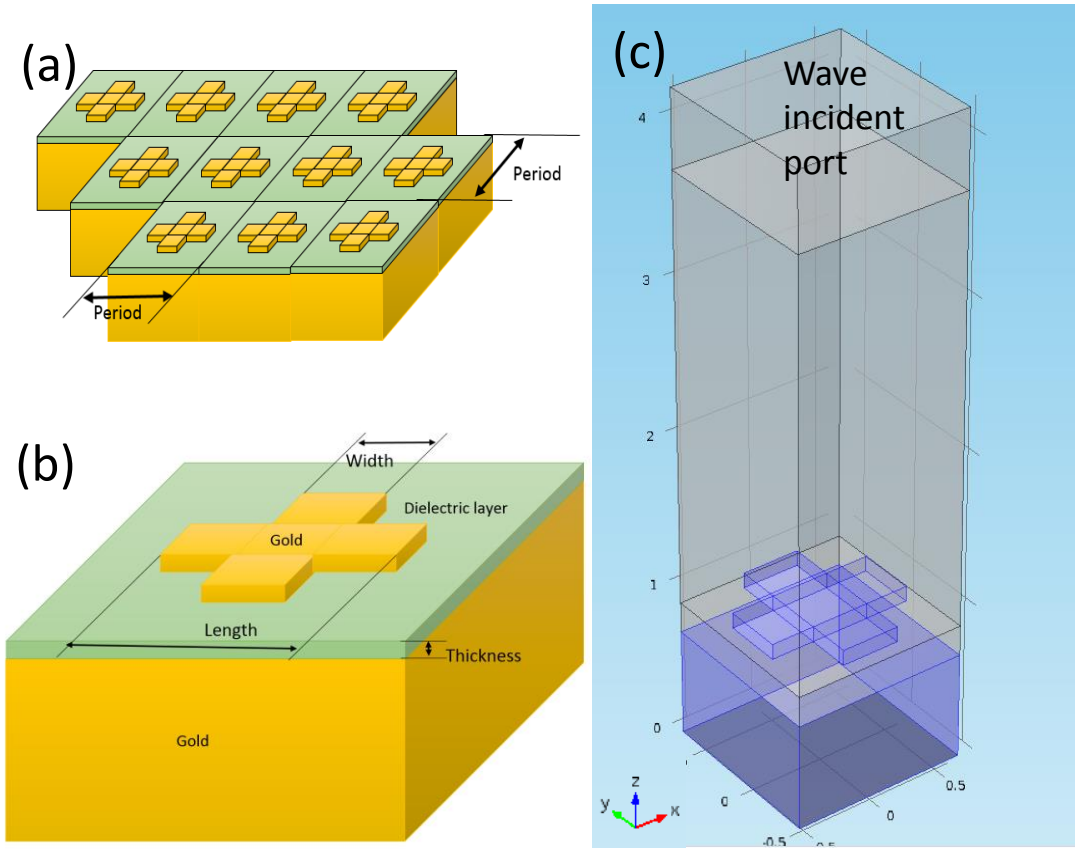

Figure 12. (a) an infinitely large array of electric ring resonators (ERR) on top of a thin dielectric layer (in green color); (b) design parameters of a ERR unit, namely, thickness of dielectric layer and length of the gold cross; (c) the simulation domain for the full wave analysis to determine the spectral absorptivity.

Characterization and design of micro-photonic devices and optical metamaterial with full wave simulations

Sy-Bor Wen, Arun Bhaskar, Vijay M. Sundaram Department of Mechanical Engineering, Texas A&M University, College Station, TX 77843

Design of perfect light absorber

Figure 13 shows the obtained absorptivity of the metamaterial with an infinitely large array of the cross-shaped ERR on the alumina under different lengths of the gold cross (c.f., figure 12a) and different thicknesses of the alumina layer. About 8000 conditions have been simulated in the batched analysis with the ADA cluster at TAMU. Each batched simulation takes about 4000 BU under parameter distributed mode parallel simulation.

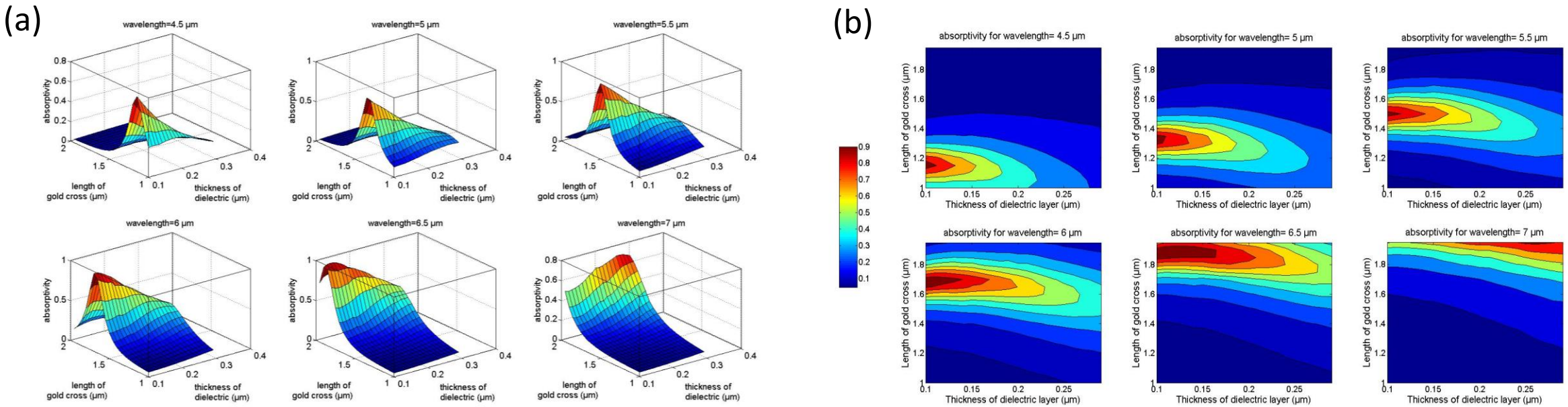

Figure 13. Absorptivity of the metamaterial at different wavelengths as functions of the size and the thickness of the Au ERR and the alumina dielectric layer. (a) Presented in 3d surface plot for wavelengths changes from 4.5 to 7μm; (b) Presented in contour plot for wavelengths changes from 4.5 to 7μm.

Characterization and design of micro-photonic devices and optical metamaterial with full wave simulations

Sy-Bor Wen, Arun Bhaskar, Vijay M. Sundaram Department of Mechanical Engineering, Texas A&M University, College Station, TX 77843

Design of perfect light absorber

Figure 14a shows the way we determined the optimized size of the Au cross-shaped ERR to be 1.9 µm and the optimized thickness of the alumina layer to be 0.12µm to achieve perfect absorptivity at λ~6.5 µm. The spectral absorptivity of such metamaterial composed with an infinite large array of Au cross-shaped ERR is illustrated in figure 14b.

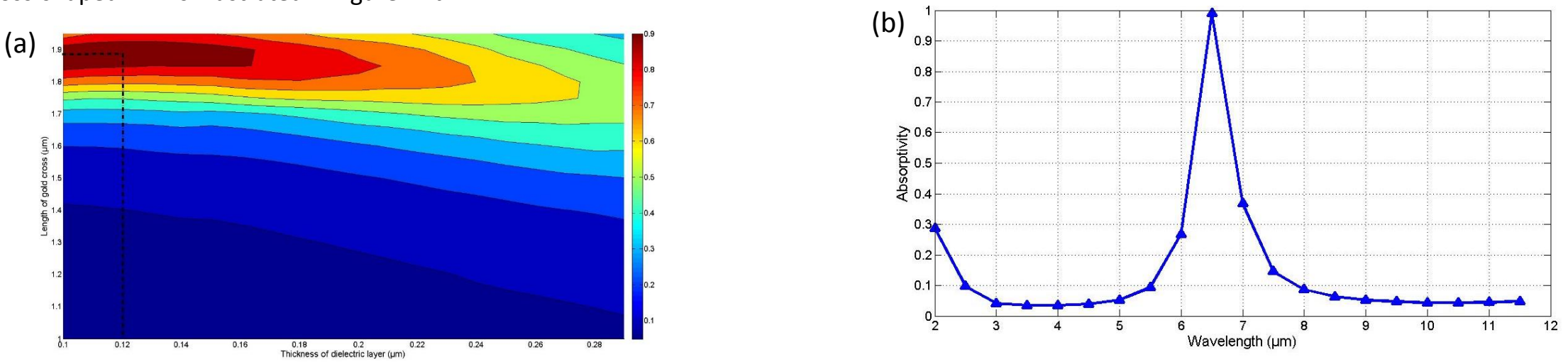

Figure 14. (a) Illustration of the procedure to obtain the dimensions of the ERR to achieve to unity absorptivity at 6.5 µm; (b) spectral absorptivity (from 2 µm to 11.5 µm) of the resulting metamaterial composed with Au ERR and alumina dielectric layer with specific size and thickness, respectively.

Acknowledgement

We acknowledge the Texas A&M Supercomputing Facility (http://sc.tamu.edu/) for providing computing resources useful in conducting the research reported here, as well as the Texas A&M AggieFab for assistances in microfabrication and imaging. We also acknowledge the assistance of Dr. Ping Luo and Mr. Derek Rodriguez of Texas A&M Supercomputing Facility for parallel simulation with COMSOL. Dr. Alok Soni and Ms. Yu Yang on the collection of direct laser machining results with NSOM .

CBET 0845794 and CBET 1545546